ACS PHYSICAL CHEMISTRY Au
AN OPEN ACCESS JOURNAL OF THE AMERICAN CHEMICAL SOCIETY

pubs.acs.org/physchemau

Article

Modeling Excited-State Proton Transfer Using the Lindblad Equation: Quantification of Time-Resolved Spectroscopy with Mechanistic Insights

Luhao Zhang, Francesca Fassioli,* Bo Fu, Zhen-Su She,* and Gregory D. Scholes*

Cite This: *ACS Phys. Chem Au* 2023, 3, 107–118

Read Online

ACCESS | Metrics & More | Article Recommendations | Supporting Information

ABSTRACT: The quantum dynamics of excited-state intramolecular proton transfer (ESIPT) is studied using a multilevel vibronic Hamiltonian and the Lindblad master equation. We simulate time-resolved fluorescence spectroscopy of 2-(2′-hydroxyphenyl) benzothiazole (HBT) and 10-hydroxybenzo[*h*]quinoline (HBQ), which suggests that the underlying mechanism behind the initial ultrafast rise and decay in the spectra is electronic state population that evolves simultaneously with proton wave packet dynamics. The results predict that the initial rise and decay signals at different wavelengths vary significantly with system properties in terms of their shape, the time, and the intensity of the maximum. These findings provide clues for data interpretation, mechanism validation, and control of the dynamics, and the model serves as an attempt toward clarifying ESIPT by direct comparison to time-resolved spectroscopy.

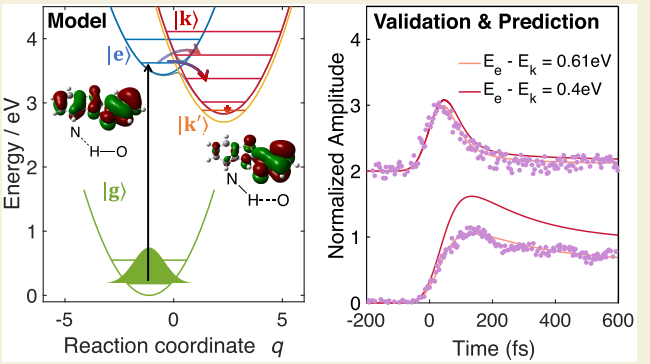

KEYWORDS: *excited-state proton transfer, quantum dynamics, Lindblad equation, ultrafast spectroscopy, electron−proton interplay*

INTRODUCTION

Excited-state intramolecular proton transfer (ESIPT) reaction is an elementary chemical reaction in which one proton is transferred with alteration of the electronic configuration in a planar molecule (Schemes 1a and S1). ESIPT reaction serves as a model system for studying the fundamental mechanism of proton transfer and has broad applications such as luminescent materials and molecular probes.[1,2] In recent years, femtosecond time-resolved spectroscopy has been used to study ESIPT in considerable detail.[3−6] Experimental investigations have shown that the proton transfer step is characterized by a universal fast rise/decay profile. A useful approach to provide physical insight into the essential mechanism and connection to the spectroscopy of chemical processes is given by the modeling of dynamics using an effective Hamiltonian that can capture the evolution of the dominant degrees of freedom encoded in the spectroscopic results. However, unlike the field of proton-coupled electron transfer (PCET),[7,8] ultrafast electron transfer,[9−11] ground-state proton transfer,[12−14] and excited-state intermolecular proton transfer,[3,15,16] in which a series of theoretical formula/models have been developed, at present, there is no general well-established model(s) for ESIPT. The complexity of ESIPT is that the pump pulse usually excites multiple skeleton vibrational modes relevant to the reaction,[17−23] suggesting the need for a nonequilibrium, multidimensional wave packet picture[19,22] with proton and electron motions coupled. This is similar to the challenges in developing a theory for photoinduced PCET reactions.[24,25] For this reason, the precise physical mechanism behind ESIPT, as well as the understanding of the initial fast rise/decay profile in spectroscopy, is still unclear. Similarly, the precise understanding of the ESIPT reaction time scale and the factors that control it would benefit from a clearer definition. Past theoretical modeling has relied on either quantum dynamics, through the evolution of electronic population and vibrational wave packet dynamics,[20,22,26] or classical molecular dynamics simulations.[27−29] In these studies, the ESIPT time scale was defined as either the characteristic time calculated from the trajectory of a combined coordinate involving H, O, N, or the period of the vibrational mode that dominates the reaction.[17,18] Here, we continue to explore the theoretical model for ESIPT, using a model with modest complexity sufficient to reproduce the time evolution of the reaction, which is consistent with time-resolved spectroscopy. On this basis, we gain insight into the ESIPT mechanism.

Received: August 18, 2022
Revised: November 21, 2022
Accepted: November 22, 2022
Published: December 21, 2022

Scheme 1. Illustration of ESIPT Reaction of HBT[a]

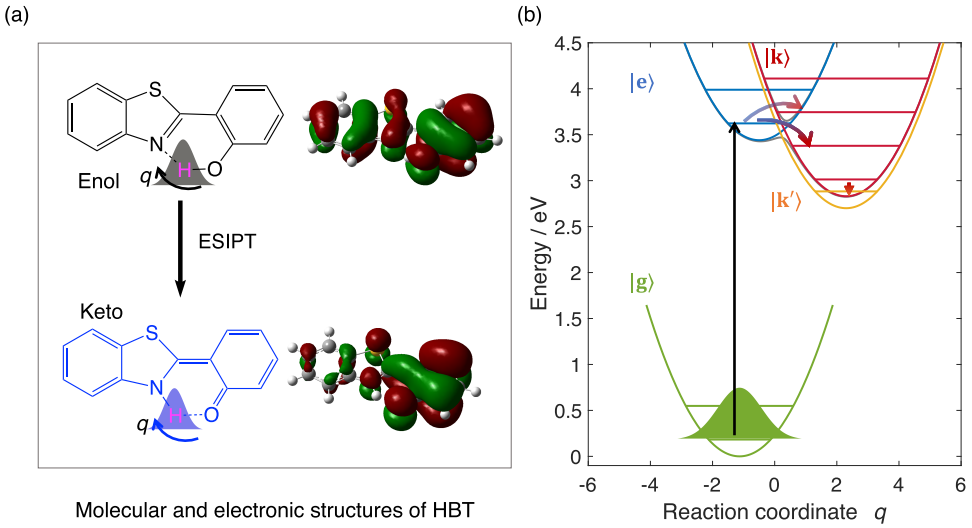

[a](a) Left: molecular structure before and after the reaction. Right: visualization of the HOMO orbital (isovalue = 0.02) of the electronic S_1 state in enol- and keto-optimized nuclear configuration. (b) Diabatic (eq 1) and adiabatic (gray line) PESs along the reaction coordinate of HBT. The arrows represent the flow of electronic population from ground to excited enol (|e⟩) states, from enol to keto (|k⟩) states, and from keto to the second keto (|k′⟩) state.

In this work, we take two widely studied molecules, 2-(2′-hydroxyphenyl) benzothiazole (HBT) and 10-hydroxybenzo-[*h*]quinoline (HBQ), as examples. For these two molecules, most ab initio simulations adopt classical full-atom molecular dynamics.[20,22,27−29] For semiclassical simulations, modeling wave packets for key degrees of freedom of nuclear motion has been done for the isolated HBQ system, and for HBT, semiclassical rate equations were adopted.[20] To take into account possible quantum dynamics arising from the interplay of electronic and nuclear degrees of freedom, as well as including the dissipation effect by the solvent environment, we use the same form of a quantum master equation for modeling both HBT and HBQ (with their isotopologues).

The outline of our paper is as follows. First, we introduce our model. Second, we develop approximated equations to calculate the time-resolved fluorescence (TRF) spectroscopy signal. Third, we compare simulation to data for both HBT and HBQ to interpret the spectra and discuss the corresponding electron−nucleus dynamics, the factors that determine the ESIPT transfer time, and the variation of TRF signals with system properties. Finally, we provide a summary of our findings and discuss future work.

METHODS

This section introduces the model and computational methods. The full dynamics of HBT/HBQ involving all electronic and nuclear degrees of freedom is intractable. We need an effective model that can capture the characteristic dynamics and offer meaningful physical insights at a modest level of complexity. Here, we adopt a reduced density-matrix approach,[30−32] in which the participating electronic states and nuclear degrees of freedom are explicitly described in the system part of the Hamiltonian. The remaining inter- and intramolecular vibrational modes of ESIPT molecules are treated as a heat bath, whose interaction with the system part is responsible for the dissipation and introduced into the quantum master equation after tracing out the bath degrees of freedom. The rest of this section will cover other assumptions and approximations made based on experimental evidence and our ESIPT model.

System Hamiltonian

The system Hamiltonian consists of the electronic part and the nuclear part. The electronic part contains four electronic states: the ground state (|g⟩), the excited enol state (|e⟩), the excited keto state (|k⟩), resulting from the electronic configuration change, which forms a new hydrogen bond, and the secondary keto state (|k′⟩) as a result of relaxation from the |k⟩ state according to the short-time (hundreds of femtosecond) red shift in spectroscopy dynamics.[17,19,33] Here, we model the observed red shift component as internal conversion, as suggested before.[34] Other possibilities include vibronic relaxation[19,35] and intramolecular vibrational redistribution (IVR).[19] In Figure S1, we simulate the case of vibronic relaxation and IVR by calculating the evolution of the probability density of an underdamped vibrational wave packet and find that the evolution of its peak position adopts the form of a damped cosine/sine function without shift; in contrast, the peak of the stimulated emission of HBT shows a significant red shift superimposing on the damped cosine/sine curve.[17] Hence, we choose to model the red shift component as the internal conversion process from a high-energy electronic state to a low-energy electronic state. As far as we are aware, there are no electronic energy structure calculations that have addressed the origin of the red shift. However, such a secondary keto state may correspond to twisted states following the planar keto state, as has been suggested for HBT in the gas phase.[28] Another possibility is that the k′ (and k) corresponds to the L_b (and L_a) state proposed in ref 34 for HBQ.

For the nuclear part, past work has proposed a skeleton deformation model for HBT,[17,18] where the main reaction coordinate is the shrinking and expansion of skeleton mode that delivers the proton, and a semi-active role of the proton for HBQ,[18,20] where both skeleton deformation and proton migration drive the reactions. Here, we choose the O−H−N as the primary coordinate, while the effect of skeleton deformation is assumed to be secondary and manifested as effective parameters in the single-coordinate model. This assumption is based on the following evidence:

First, several first-principles calculations have confirmed that there is a single S1 PES that connects the enol species and keto species[20,29] so that the relaxation of the molecule on the S1 PES from the enol geometry to the keto geometry causes the difference between enol absorption, enol fluorescence, and keto fluorescence. The energy difference between the enol and keto minimum in the excited state is around 0.45 eV[18] (see Definition of Parameters) in HBT. Due to the significant geometry change associated with proton transfer, most of

https://doi.org/10.1021/acsphyschemau.2c00038
ACS Phys. Chem Au 2023, 3, 107−118

this difference should be caused by relaxation along the reaction coordinate. However, the oscillation range of the transient absorption spectrum intensity along different wavelengths (Figure 2 in ref 17), which can be translated into the relaxation energy of the skeleton mode wave packet caused by enol−keto electronic transition, is only around 0.07 eV (for details of estimation, see the Supporting Information). Therefore, we judge that it is unlikely that the skeleton mode is the reaction coordinate and that it is instead the H−O−N coordinate that makes a significant contribution to the molecules' relaxation energy from the enol minimum to keto minimum geometry.

Second, if a skeleton wave packet moving toward the keto PES minimum corresponds to the fast rise of the keto signal as proposed in previous work,[17] the dynamics would have given the same maximum intensity of the initial fast rise (the maximum of the nonoscillatory part) in the signals at different keto wavelengths (e.g., $\lambda > 500$ nm in ref 17), corresponding to the peak of the wave packet scanning along different positions of the PES. However, this is not observed in the experimental spectra.[17]

Third, in the two-dimensional PESs' calculations of the two molecules using TDDFT,[20] during the minimal energy paths from the Franck−Condon point to the keto energy minimum, the distance traveled by the O−H coordinate (R(OH)), which represents free hydrogen migration, is larger than the distance traveled by the O−N coordinate (R(ON)), which represents skeleton deformation. For HBT, R(OH) is ∼0.76 Å and R(ON) is only ∼0.33 Å. For HBQ, R(OH) is ∼0.70 Å and R(ON) is only ∼0.30 Å.

Finally, previous work[22] used the skeleton deformation model (dynamics of enol−keto transition is controlled by skeleton mode vibration) but gained multistage dynamics inconsistent with the continuously changing trace in the TRF spectra.

The solvent coordinate is not explicitly modeled as is in proton-coupled electron transfer reactions[36] because the solvent effect is not observed.[18]

Guided by these considerations, the molecular part of the system Hamiltonian is written as a molecular vibronic coupling Hamiltonian,[37−39]eq 1. This approach is widely used in the context of ultrafast photoinduced processes, e.g., electronic energy transfer, electron transfer, and proton-coupled electron transfer reaction.[7,40−45] It is noted that conceptually similar models of other ESIPT molecules were proposed by May and collaborators[26] for a double-site molecule 2,5-bis(2-benzoxazolyl)-hydroquinone, and consistency with the fluorescence excitation spectrum was obtained that pointed out to a double-transferred product.

$$\begin{aligned}\hat{H}_m(\hat{p},\hat{q}) = {} & \frac{\hbar\omega}{2}\hat{p}^2 \otimes \mathbb{I}_{ele} + \left[\frac{\hbar\omega}{2}(\hat{q}-\delta_g)^2 + E_g\right] \\ & \otimes |g\rangle\langle g| + \left[\frac{\hbar\omega}{2}(\hat{q}-\delta_e)^2 + E_e\right] \\ & \otimes |e\rangle\langle e| + \left[\frac{\hbar\omega}{2}(\hat{q}-\delta_k)^2 + E_k\right] \\ & \otimes |k\rangle\langle k| + \left[\frac{\hbar\omega}{2}(\hat{q}-\delta_{k'})^2 + E_{k'}\right] \otimes |k\rangle\langle k'| \\ & + V|e\rangle\langle k| + V|k\rangle\langle e| \end{aligned} \quad (1)$$

$\hat{q} \equiv \left(\frac{m\omega}{\hbar}\right)^{1/2}\hat{Q}$ and $\hat{p} = (m\omega\hbar)^{-1/2}\hat{P}$ are the position and momentum operators of the dimensionless proton coordinate, respectively, where $\hat{P}$ and $\hat{Q}$ are their real-space counterparts. We assume that the diabatic potential energy surface (PES) associated with each diabatic state, as shown in Scheme 1, is harmonic and shares the same vibrational frequencies ω, with δ_i (i = g, e, k, k′) defined as the local minimum of diabatic state $|i\rangle$. An electronic coupling V between $|e\rangle$ and $|k\rangle$ is responsible for the electronic transition $|e\rangle \leftrightarrow |k\rangle$. In principle, the coupling V comes as a function of proton coordinate q. As is often the case in the literature,[39] here, we adopt a zero-order approximation by assuming that V is independent of the nuclear coordinates (see detailed discussion in the Supporting Information).

We furthermore introduce the radiation−matter interaction $\hat{H}_{int}$ given in terms of the dipole approximation as

$$\hat{H}_{int} = -\hat{\mu}\bullet\hat{\epsilon}\mu E(t)(|e\rangle\langle g| + |g\rangle\langle e|) \quad (2)$$

Here, $\hat{\mu}$ and μ are, respectively, the unit vector and the norm of the transition dipole moment for electronic transition $|g\rangle \leftrightarrow |e\rangle$, which is assumed to be independent of the vibrational coordinates (Condon approximation). We assume that only $|e\rangle$ couples $|g\rangle$ through light-matter interaction and $|k\rangle$ is a dark state based on the fact that there has been no evidence showing ground enol species being excited to keto. Therefore, the system could be prepared at its enol configuration upon photoexcitation.

The electric field $\hat{\epsilon}\cdot E(t)$ at the position of the molecule is given as

$$\hat{\epsilon}\bullet E(t) = \hat{\epsilon}\bullet\epsilon(t)\cos\omega_p t, \quad \epsilon(t) = I \times e^{(-(t^2/2\tau^2))} \quad (3)$$

where $\hat{\epsilon}$ is the unit polarization vector, $\epsilon(t)$ is a Gaussian-shape pulse envelope function, and ω_p is the center frequency of the pump pulse. As in typical experiments,[17] $\mu E(t)$ in this paper is set on a much smaller scale compared to $E_e - E_g$ so that the light acts as a perturbation. We set $t = 0$ as the moment when the maximum pump pulse reaches the position of the molecule. Then, the total system Hamiltonian is $\hat{H}_s = \hat{H}_m + \hat{H}_{int} \otimes \mathbb{I}_q$, where $\mathbb{I}_q$ is the identity operator of the vibrational subspace.

Equations of Motion for Reduced Density Operator $\hat{\rho}$

To account for the interaction between the molecular system and a larger number of environmental degrees of freedom, we use a Markovian quantum master equation approach, the Lindblad master equation[31,46,47](eq 4). The Lindblad master equation preserves all of the properties of the density matrix (trace-preserving and completely positive) by assuming weak coupling between the system and a Markovian bath within the rotating wave approximation. It enables us to model desired dynamics phenomenologically,[48] where the Lindblad operator in eq 4 could be constructed accordingly.[32] The details of the form of the Lindblad equation used here are shown below

$$\begin{aligned}\frac{d\hat{\rho}(t)}{dt} &= -\frac{i}{\hbar}[\hat{H}_s, \hat{\rho}(t)] + \mathcal{D}(\hat{\rho}(t)) \\ \mathcal{D} &= \sum_i \gamma_i\left(A_i\hat{\rho}A_i^\dagger - \frac{1}{2}\{A_i^\dagger A_i, \hat{\rho}\}\right)\end{aligned} \quad (4)$$

$\mathcal{D}$ is the dissipator that can include several dissipation effects caused by the system-bath coupling through the action of the operator A_i that acts on the system density matrix $\hat{\rho}$. Damping of the vibrational mode takes the form of the damped harmonic oscillator model,[31] where the Lindblad operators are given by a summation of single vibrational creation/annihilation operators associated with each excited diabatic state ($|e\rangle$, $|k\rangle$, $|k'\rangle$)

$$\begin{aligned}\hat{A}_1 &= \sum_{j=e,k,k'} |j\rangle\langle j| \otimes \hat{a}_j,\ \hat{a}_j \equiv \hat{a} - \frac{\delta_j}{\sqrt{2}},\ \gamma_1 = \gamma_{mode}(1+\bar{n}(T)) \\ \hat{A}_2 &= \sum_{j=e,k,k'} |j\rangle\langle j| \otimes \hat{a}_j^\dagger,\ \hat{a}_j^\dagger \equiv \hat{a}_j^\dagger - \frac{\delta_j}{\sqrt{2}},\ \gamma_2 \\ &= \gamma_{mode}\bar{n}(T)\end{aligned} \quad (5)$$

The damping parameter γ_{mode} is related to the spectral density at the system modes' frequency, $\gamma_{mode} = 2J(\omega)$.[49] $\bar{n}(T) = 1/(e^{\hbar\omega/k_BT} - 1)$ is the averaged quanta of the vibrational mode. k_B is the Boltzmann constant. $\hat{A}_1$ is responsible for the energy dissipation from the system to the environment, while $\hat{A}_2$ leads to the excitation of the system by the environment, where $\frac{\gamma_1}{\gamma_2} = e^{\hbar\omega/k_BT}$ guarantees detailed balance within a single electronic PES. This form (also termed diabatic damping approximation in Redfield theory) has also been used to model dissipation in electron transfer reactions with multiple states.[9] It is discussed in the literature[50] that the Lindblad master equation with a local basis does not lead to thermalizations that follow the

https://doi.org/10.1021/acsphyschemau.2c00038
ACS Phys. Chem Au 2023, 3, 107−118

Boltzmann distribution. In the parameter regime of our model, the electronic coupling V is small compared to the energy gap between $|e\rangle$ and $|k\rangle$ electronic states so that $\hat{A}_{1/2}$ on the local basis ($|e\rangle$, $|k\rangle$, $|k'\rangle$) without the off-diagonal term should be a good approximation, so the Boltzmann equilibrium is approximately satisfied with realistic reaction yield. In the regime we simulate, the vast majority of the ground electronic population is at the vibrational ground state; thus, the damping effect of the vibrational mode on the ground electronic state is neglected.

In addition, as mentioned before, to describe the internal conversion process for spectroscopy redshift, we include Lindblad operators that lead to transitions between a higher and a lower electronic keto state, $|k\rangle \leftrightarrow |k'\rangle$

$$\begin{aligned}\hat{A}_3 &= |k\rangle\langle k'| \otimes \mathbb{I}_{vib},\ \gamma_3 \\ &= \gamma_R \hat{A}_4 = |k'\rangle\langle k| \otimes \mathbb{I}_{vib},\ \gamma_4 = e^{(E_k - E_{k'})/k_B T}\gamma_R\end{aligned} \tag{6}$$

where γ_R is the electronic relaxation parameters and the population distribution on $|k\rangle$ and $|k'\rangle$ states will follow Boltzmann distribution. The initial state is then set as a product of the ground electronic state and the vibrational thermal state

$$\hat{\rho}(0) = |g\rangle\langle g| \otimes \sum_{n=1,2,\cdots,N} \frac{e^{(E_n - E_0)/k_B T}}{\sum_m e^{(E_m - E_0)/k_B T}} |n\rangle\langle n| \tag{7}$$

Calculation of Time-Resolved Fluorescence (TRF)

Single-wavelength TRF traces typical of ESIPT reactions show a rise-decay profile superimposed with an oscillating signal that is interpreted as low-frequency mode vibration.[20] It is thought that wave packets produced by impulsive excitation of the low-frequency modes evolve independently from the reaction (i.e., proton motion and electron configuration change).[51,52] Here, we focus on studying the spectroscopy of the proton transfer stage, i.e., the initial rise and decay of the trace. Hence, we derive a simplified formula of the nonoscillating contribution to the TRF profile based on the results of perturbation theory[53] with two physical assumptions: first, the actual width of the gate pulse is assumed to be several times shorter than that of the pump pulse in the experiment and second, we assume that the excited-state dynamics of the wave packet along the proton coordinate is static. A detailed derivation is presented in the Supporting Information. We find that the nonoscillating TRF profile, $\overline{S}_{st}(t,\omega)$, is approximated by a combination of several dynamically evolving components associated with the $|e\rangle$, $|k\rangle$, $|k'\rangle$ electronic states, and the dynamical amplitude of each component is proportional to the population dynamics of each electronic state. That is indicated by eq 8

$$\overline{S}_{st}(t,\omega) = \sum_{i=e,k,k'} c_i(\omega) P_i(t) \tag{8}$$

where $c_i(\omega)$ is a wavelength-dependent TRF coefficient that characterizes the spectroscopy line shape of each component. $\overline{S}_{st}(t,\omega)$ represents the TRF signal of the excited-state photophysics. This simplification of the total signal makes the interpretation of spectroscopy more intuitive. We justify in the following result section that this approximation is reasonable.

Definition of Parameters

The values of the parameters specifying the model for the HBT and HBQ systems are collected in Table S1. ω_{OH} for the diabatic electronic state is obtained by calculating the ground-state OH stretching frequency of HBT and is kept the same for HBQ.

$\delta_{q,e} - \delta_{q,g}$ characterizes the enol reorganization energy from the ground to enol states along OH mode. There is no vibronic progression observed in absorption spectroscopy, so a good estimate of $\delta_{q,e} - \delta_{q,g}$ cannot be determined in this way. This indicates two possibilities: the first case is that OH mode contributes only slightly to the total enol reorganization energy compared to the other $3N - 7$ modes (N being the number of atoms in a molecule); the second case is that OH mode dominates the total enol reorganization energy so that the absorption spectroscopy peak is the 0−1 transition along OH mode based on HBT absorption and emission spectroscopy in ethanol,[17] and the peak energy is expected to vary with deuteration. Quantum chemistry calculation shows that the Franck−Condon transition from the enol ground state excites a broad spectrum of normal modes;[21] here, we choose the first case and set $\delta_{q,e} - \delta_{q,g} = 0.63$ for both HBT and HBQ, representing a small enol reorganization energy along OH mode. It is shown in Figure 6f that when changing $\delta_{q,e} - \delta_{q,g}$, only the total intensity of the TRF traces is affected, which of course is irrelevant to the normalized data. Thus, we do not require an accurate estimation of $\delta_{q,e} - \delta_{q,g}$ here.

E_e is the minimum of the enol state ($|e\rangle$) PES in eq 1 and is set to the pump center energy such that the 0−0 transition along OH mode resonates with the pump pulse. This resonating excitation population dynamics with a single OH mode is assumed proportional to the resonating excitation population dynamics of a system with a complete set of modes, so the current reduced single OH mode model is a good representation of the complete system, and E_e is effective energy equal to the summation of minimum energy in the realistic multidimensional PES and the vibrational energy of the eigenstate of all other modes.

Then, we identify parameters related to laser fields employed in the simulation. As in the experiment, the center wavelength of the pump pulse used in the calculation is 360 nm for HBT and 390 nm for HBQ.[18] The FWHM of the pump is set so that the simulated rise in the enol signal is consistent with the data and is fixed when simulating other wavelengths. The amplitude of pump envelope I, its polarization, and the dipole moment are chosen so that the total excited population is on the scale of 1%, as estimated in the experiment.[17]

The parameters associated with keto diabatic PES are determined with the guidance of optical information, literature report, and quantum chemistry calculations: $E_e - E_k$ is the enol−keto energy gap on excited states, which we estimate from the energy difference between enol fluorescence and keto fluorescence, and depends on the difference in energy between the enol and keto forms in both the excited and ground states. The ground-state energy change from enol to keto is usually of the same order of magnitude as the energy change in the excited state (with the keto ground-state energy being above the enol ground-state energy). Consequently, the energy difference between the excited-state enol and keto minimum can be roughly approximated by half the difference in enol and keto fluorescence (this is, ∼0.45 eV for HBT[17,18] and ∼0.49 eV for HBQ[20]). V is on the same scale as electronic couplings in ultrafast photoinduced electron transfer reactions[43,44,54](e.g., 0.03 eV[43]). $\delta_{q,k} - \delta_{q,e}$ is an effective hydrogen migration length under the harmonic approximation for the diabatic potential energy surface (PES) and includes the skeleton deformation effect. On the one hand, the initial skeleton relaxation shortens the H−N distance and makes the $\delta_{q,k} - \delta_{q,e}$ smaller than the distance between the enol Franck−Condon geometry and the keto minimum energy geometry (∼7 in dimensionless coordinate, see detailed calculation in the Supporting Information). On the other hand, because hydrogen migrates from the O atom to the N atom far from the equilibrium position of OH/ON vibration, the diabatic PES should be flatter (anharmonic) as hydrogen moves away from the O/N atom. Under the harmonic approximation of enol and keto diabatic PES, the corresponding effective hydrogen migration length is further shortened. Under these constraints, we chose these parameters to optimize the agreement of the calculated TRF profile (both yield and transfer rate) with the experimental data at an enol-dominated wavelength and fix the parameters for the calculation of the keto-dominated wavelength.

Let us finally turn to the energy difference between the keto state and the relaxation state $|k'\rangle$. $E_k - E_{k'}$ is determined from the peak shift of the short-time red shift dynamics in pump−probe spectroscopy of HBT and HBQ.[17,19] The relaxation rate constant, γ_R, is chosen so that the decay stage of the simulated TRF signal matches the ∼300 fs decay profile of data after fast transfer.

When simulating the deuterated isotopologues, all parameters are fixed to be the same as the original species, except for the proton/

https://doi.org/10.1021/acsphyschemau.2c00038
ACS Phys. Chem Au 2023, 3, 107−118

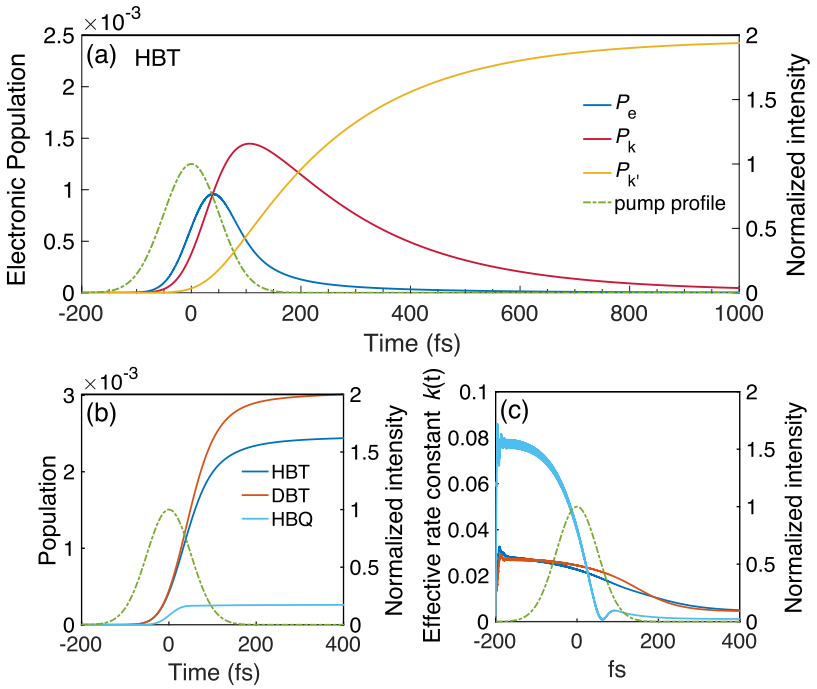

Figure 1. Electronic excitation-transfer−relaxation dynamics of HBT and HBQ ESIPT. Panel (a) shows the population on all three electronic excited states, $|e\rangle$, $|k\rangle$, and $|k'\rangle$, of HBT. Panel (b) shows the accumulation of product state population. Panel (c) shows the effective time-dependent first-order kinetic rate coefficient from enol to keto(keto') transfer.

deuteron mass. For vibrational frequency, $\omega_{OD} = \frac{\omega_{OH}}{\sqrt{2}}$ is based on the $\omega = \sqrt{\frac{k}{m}}$ of the harmonic oscillator. γ_{mode} is fixed to 0.1/fs for both HBT and HBQ, assuming a similar dissipation environment of the N···H···O and the benzene ring system. When substituting H by D, γ_{mode} is assumed to be inversely proportional to the effective mass of the vibration, $\frac{\gamma_{mode,H}}{\gamma_{mode,D}} = 2$, with spectral density $J(\omega) \equiv m_{vib}\gamma\omega$.[55] See the Supporting Information for detailed derivation. The displacements in dimensionless coordinates are all scaled by $\left(\frac{m_H}{m_D}\right)^{1/4}$ after deuteration.

Computational Details

We propagate the Lindblad equation (eq 1) numerically using a low-storage Runge−Kutta method,[56] with time step = 0.02 fs and stage number = 1. $\hat{H}_m$ and $\hat{H}_{int}$ are presented on a direct product basis: $|n,i\rangle \equiv |n\rangle \otimes |i\rangle$, n = 0, 1, 2,···, N, i = g, e, k, k′. $|i\rangle$ indexes the four electronic states, and $|n\rangle$ is the centered harmonic-oscillator basis states with frequency ω. We use N = 25 for HBT and N = 20 for HBQ in this paper for converged results. The total density matrix $\hat{\rho}(t)$ then has the dimension $4N \times 4N$

$$\hat{\rho}(t) = \sum_{i,j=g,e,k,k'} \sum_{n,m=0,1,2,\cdots,N} |n, i\rangle \rho^{ij}_{n,m}(t) \langle m, j| \tag{9}$$

$\hat{\rho}^{ij}$ is the block electronic density matrix associated with the ith and jth electronic state ($N \times N$ dimension)

$$\hat{\rho}^{ij}(t) = \sum_{n,m=0,1,2,\cdots,N} |n\rangle\langle n, i|\hat{\rho}(t)|m, j\rangle\langle m| \tag{10}$$

The electronic population of each state, P_i, is given by

$$P_i = \sum_{n=1,2,\cdots,N} \langle n, i|\hat{\rho}(t)|n, i\rangle \equiv \mathrm{Tr}_{vib}[\hat{\rho}^{ii}(t)] \tag{11}$$

Equation 11 then sums up all of the diagonal terms (population on each vibronic basis) of $\hat{\rho}^{ii}$.

Vibrational frequency calculation for OH mode and calculation for H migration distance (change of OH distance from the Franck−Condon geometry to keto minimum geometry, 0.74 Å) were carried out using the DFT method for the ground state and TDDFT methods for the excited state at the M06/cc-PVDZ level by Gaussian 16.[57] Orbital wavefunction visualization was carried out by GaussView 6.[58]

RESULTS

Excitation-Transfer−Relaxation Dynamics

To have an understanding of the global features of dynamics among ground, enol, keto, and keto' states, using parameters defined above, we performed numerical simulations of the system density matrix, $\hat{\rho}(t)$, and obtained electronic population on $|e\rangle$, $|k\rangle$, and $|k'\rangle$ states, P_e, P_k, and $P_{k'}$, using eq 11. The results for HBT are shown in Figure 1a. We see clearly that the rise of P_e is delayed beyond the rise of the pump field. P_k rises more delayed than P_e but initially grows together with P_e. The peak of P_k is not equal to but higher than that of P_e. $P_{k'}$ rises the latest and provides the dominant contribution to the signal in the end.

Figure 1b presents the accumulation of product state population. $P_{k,k'} = P_k + P_{k'}$ represents the overall monotonic reaction process from excitation to product for a specific system condition, which includes two aspects, the absolute accumulation and the accumulation time. The absolute accumulation of the DBT population is quicker than HBT, and the final population is higher. But for the accumulation time to reach saturation, the two species are similar, consistent with the similar fitted transfer time in the relevant experimental paper.[18] For HBQ under a shorter pump duration, the accumulation amount is less than HBT, but the accumulation time of HBQ is shorter than HBT. Therefore, we see that the absolute accumulation is sensitive to system conditions (like deuteration) besides the fitted transfer time gained from normalized spectroscopy.

It has been questioned whether the enol to keto transformation is a rate-governed process. In experimental studies,

https://doi.org/10.1021/acsphyschemau.2c00038
ACS Phys. Chem Au 2023, 3, 107−118

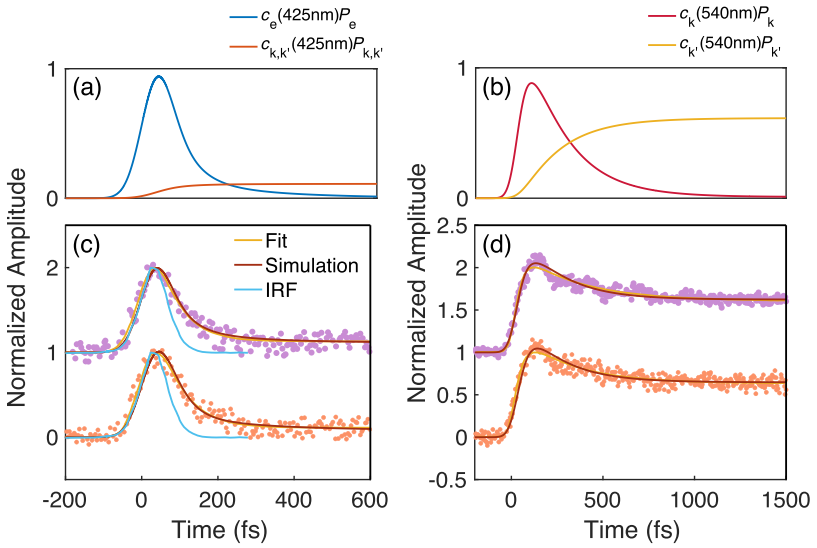

Figure 2. Simulation of HBT spectroscopy and their deuterated species. (a, b) are the corresponding spectroscopy components ($c_iP_i(t)$ in eq 8) in HBT at 425 and 540 nm, respectively. (c, d) are the simulated TRF profiles (red line) compared with the experiments (dots) and the fittings (yellow line) of HBT (purple dot) and DBT (orange dot) at 425 and 540 nm, respectively. The light blue line is the instrumental response function (IRF). Adapted with permission from ref 18. Copyright 2022 American Chemical Society.

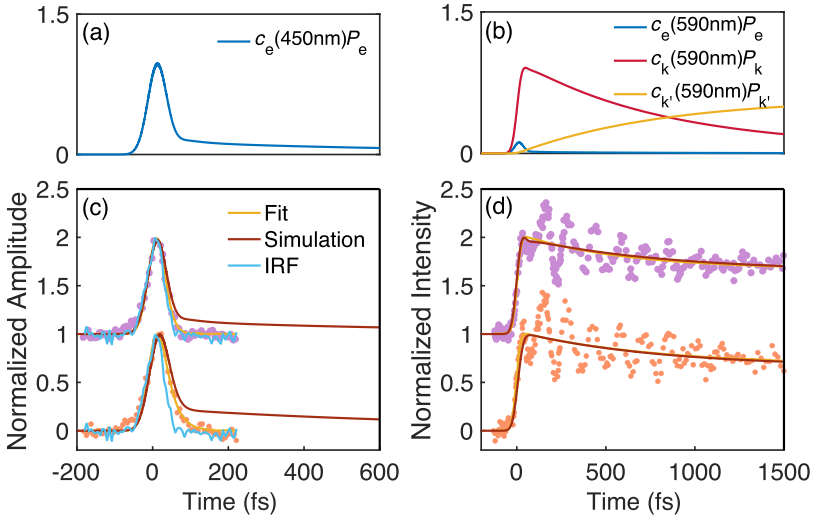

Figure 3. Simulation of HBQ spectroscopy and their deuterated species. (a, b) are the corresponding spectroscopy components ($c_iP_i(t)$ in eq 8) in HBQ at 450 and 590 nm, respectively. (c, d) are the simulated TRF profiles (red line) compared with the experiments (dots) and the fittings (yellow line) of HBQ (purple dot) and DBQ (orange dot) at 450 and 590 nm, respectively. The light blue line is the instrumental response function (IRF). Adapted with permission from ref 18. Copyright 2022 American Chemical Society.

an exponential function is generally used to fit the excited-state dynamics,[18,19,23,59,60] but some work has argued that this is not the case.[17] We look closer at the dynamics of the proton transfer stage by calculating the effective time-dependent first-order kinetic rate coefficient numerically from enol to keto(keto') transfer: $k(t) \equiv \frac{dP_{k,k'}(t)}{dt} \bullet \frac{1}{P_e(t)}$, dt = 0.02 fs, and plotting it in Figure 1c. It shows that for both HBQ and HBT, the rate coefficient varies with time and is not a constant, and apparently, HBQ overall has a faster $k(t)$. The time-dependent behavior of $k(t)$ indicates that the reaction process cannot be described simply by a transport that obeys the Fermi-golden rule and suggests that nonequilibrium quantum dynamics may be at play, though mathematically, the spectroscopy profile can be constructed using multiple exponential functions.

Simulation and Interpretation of Ultrafast Spectroscopy

To verify our simulation and provide more interpretation of the dynamics behind the characteristic fast rise/decay profile of HBT and HBQ spectroscopy, we apply eq 8 to calculate the TRF signal of the excited-state photophysics of HBT, HBQ, and their deuterated species. First, we analyze the corresponding excited-state species at each selected wavelength. For HBT, the 425 nm TRF signal shows a long-time residue, so we infer that the 425 nm trace (S_{st} (425 nm)) is dominated by an enol signal and a bit of keto spectroscopy tail, while the 540 nm trace (S_{st} (540 nm)) is at the peak of keto fluorescence with little overlap with enol fluorescence[17] and is thought to be purely a keto signal. Then, the TRF equation of the excited-state photophysics of HBT is expressed as S_{st} (425 nm,t) = $c_e^{425\ nm}P_e(t)$ + $c_{k,k'}^{425\ nm}[P_k(t)$ + $P_{k'}(t)]$, assuming the same emission coefficient, $c_{k,k'}^{425,nm}$, for both keto and keto' states; S_{st}

https://doi.org/10.1021/acsphyschemau.2c00038
ACS Phys. Chem Au 2023, 3, 107−118

$(540\ \text{nm},t) = c_{k}^{540\ \text{nm}} \times P_{k}(t) + c_{k'}^{540\ \text{nm}} \times P_{k'}(t)$. For HBQ, it is clear that the 450 nm trace decays to zero and therefore is purely an enol signal. For the 590 nm trace, due to the similarity and slight difference of its initial fast rise with those at 450 and 520 nm (see Figure 2 of ref 18), we assume that it is mainly the keto signal but mixed with some enol signal. The TRF equation of the excited-state photophysics of HBQ is S_{st} $(450\ \text{nm},t) = c_{e}^{450\ \text{nm}} \times P_{e}(t)$; S_{st} $(590\ \text{nm},t) = c_{e}^{590\ \text{nm}} \times P_{e}(t) + c_{k}^{590\ \text{nm}} \times P_{k}(t) + c_{k'}^{590\ \text{nm}} \times P_{k'}(t)$.

Applying the above equations to calculate the TRF signal of the excited-state photophysics for HBT (Figure 2c,d) and HBQ (Figure 3c,d) with emission coefficients in Table 1, we obtain results consistent with the nonoscillating part of experimental data as well as the fitting function reported in ref 18. Figures 2a,b and 3a,b show the components, $c_i P_i(t)$ of enol and keto (keto') states that construct the total profiles at selected wavelengths. The consistency between simulation and TRF data supports our parameter choice and model and indicates that the physical process corresponding to the fast rise/decay is the evolution of the reactant and product electronic population. The consistency also provides a physical explanation for different values of the fitted transfer time at different wavelengths that are generally observed in ESIPT spectroscopy,[19,20] like 425 nm (62 fs) and 540 nm (47 fs) in Figure 2 using a multiple exponential fit.[18] Our model suggests that the difference in transfer times with wavelength may come from a coupled nonequilibrium excitation-transfer−relaxation process that results in a wavelength-dependent combination of multiple components that have different characteristic times. For example, in Figure 1a, the rise of keto' $(P_{k'}(t))$ population is the slowest, and the decay of the enol population $(P_{e}(t))$ is slower than the rise of the keto population $(P_{k}(t))$. This may contribute to a slower decay at 425 nm that is dominated by enol species in contrast to the faster rise at 540 nm that is dominated by keto species.

As we have mentioned, past work has hypothesized that HBT ESIPT is promoted by heavy skeleton modes[18] and HBQ by a semi/full-active proton;[18,20] however, this picture does not fully explain the experimental observations. The agreement between our simulated TRF spectra, based on a model where the O−H mode is the dominant reaction, and the experimental spectra suggests instead that both the HBT and HBQ reactions may be mainly driven by the OH mode rather than the low-frequency skeleton modes. It also suggests that the oscillation pattern in Figures 2 and 3, likely arising from the skeleton mode vibration, which has not been explicitly modeled in this work, is only adding amplitude modification to the main

Table 1. Emission Coefficients of Enol and Keto States of HBT(DBT) and HBQ(DBQ) in Figures 1 and 2

	$c_{e}^{425\ \text{nm}}$	$c_{k,k'}^{425\ \text{nm}}$	$c_{k}^{540\ \text{nm}}$	$c_{k'}^{540\ \text{nm}}$
HBT	9.8×10^{2}	4.5×10^{1}	6.1×10^{2}	2.5×10^{2}
DBT	9.3×10^{2}	2.6×10^{1}	4.8×10^{2}	2.1×10^{2}
	$c_{e}^{450\ \text{nm}}$	$c_{e}^{590\ \text{nm}}$	$c_{k}^{590\ \text{nm}}$	$c_{k'}^{590\ \text{nm}}$
HBQ	7.5×10^{3}	0.9×10^{3}	3.9×10^{3}	2.3×10^{3}
DBQ	4.9×10^{3}	1.0×10^{3}	1.3×10^{3}	0.8×10^{3}

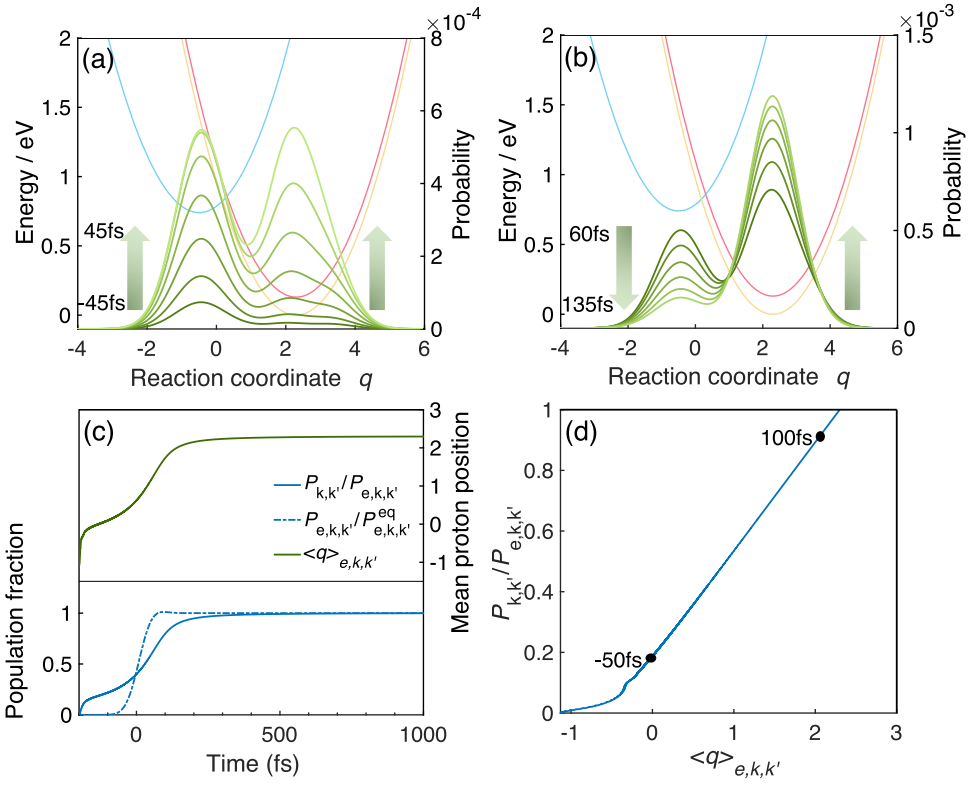

Figure 4. Dynamics of electron and OH vibration during ESIPT of HBT. (a, b) Proton wave packet density on excited states from −45 to 45 fs and 60 to 135 fs. The enol, keto, and keto' PESs are in light blue, light red, and light orange, respectively. (c). Product electronic fraction in the total population on the excited state (blue, solid line): $P_{k,k'}/P_{e,k,k'}$, and normalized total population on the excited state (blue, dashed line): $P_{e,k,k'}(t)/P^{eq}_{e,k,k'}$. The mean position of the total proton wave packet on the excited state (green line): $\langle q \rangle_{e,k,k'}$. (d). Correlation between electron and proton degrees of freedom of the excited state.

https://doi.org/10.1021/acsphyschemau.2c00038
ACS Phys. Chem Au 2023, 3, 107−118

profile. To gain insight into the underlying electronic state dynamics, we plot the time evolution of the reactant and product populations in Figure 1c. It shows that the enol−keto electronic transition takes place immediately ($k(t)$ grows immediately) when the enol population begins to accumulate and lasts several hundreds of femtoseconds, instead of a sudden "electronic switch" induced by nuclei moving adiabatically across the transition state configuration as thought before.[22]

Wave Packet Dynamics and Electron−Nucleus Correlation

To gain further physical insight into the transfer mechanism suggested by the model, we track the proton wave packet dynamics and analyze its relationship with electronic dynamics. In Figure 4a,b, we plot the total proton wave packet density on the excited state. It shows an increase of both enol and keto wave packets during ∼−45 to 45 fs (see Figure S2 for plotting enol and keto(keto') separately) and a decaying enol contribution with increasing keto population after ∼60 fs. An apparent feature is a static wave packet on both enol and keto diabatic PES, consistent with the fact that there are no high-frequency oscillations on the initial fast rise/decay profile in spectroscopy and in the assumption in deriving eq 8. Recent ab initio calculation of HBT's proton density shows a decrease of the density peak in O atom vicinity and growth of the density peak in N atom vicinity,[28] which is consistent with Figure 4a,b. In Figure 4c, we plot the product electronic fraction, $P_{k,k'}$, in the total population on the excited state, $P_{e,k,k'}$: $\frac{P_{k,k'}}{P_{e,k,k'}}$, $P_{k,k'} \equiv P_k + P_{k'}$, $P_{e,k,k'} \equiv P_e + P_k + P_{k'}$. It evolves from 0 to 1. For comparison, we also plot $P_{e,k,k'}$. For the proton, we plot the mean position of the total proton wave packet in Figure 4a,b, $\langle q \rangle_{e,k,k'}$ (eq 12), which evolves from the ground state local minimum to enol local minimum and to keto local minimum

$$\langle q \rangle_{e,k,k'} = \frac{\frac{1}{\sqrt{2}}\mathrm{Tr}_{vib}[(\hat{a}^\dagger + \hat{a})(\hat{\rho}^{ee}(t) + \hat{\rho}^{kk}(t) + \hat{\rho}^{k'k'}(t))]}{P_e(t) + P_k(t) + P_{k'}(t)} \quad (12)$$

$\hat{\rho}^{ii}$ is the block density matrix of the ith state. Then, in Figure 4d, we plot the correlation between the electron and proton degrees of freedom of the excited state. A linear correlation (after −50 fs when the excited state has observable accumulated population) shows that the electron configuration and proton evolve synchronously, which may come from the proton wave packet being delocalized and quickly dephasing to equilibrium (Figure 4a,b). These results provide a new alternative to the previously accepted reaction mechanism where the electronic configuration undergoes a sudden transition when the local nuclear wave packet crosses the diabatic PESs, a scenario under which the electron−proton correlation would instead be step-like. To gain further insight into how electronic population and proton motion are correlated, we analyze the evolution of the proton mean position under different enol−keto electronic coupling values V in Figure 5a and find that the proton evolves faster with larger V, pointing toward the importance of the nonadiabatic coupling V in controlling the dynamics under the regime and assumptions in our model.

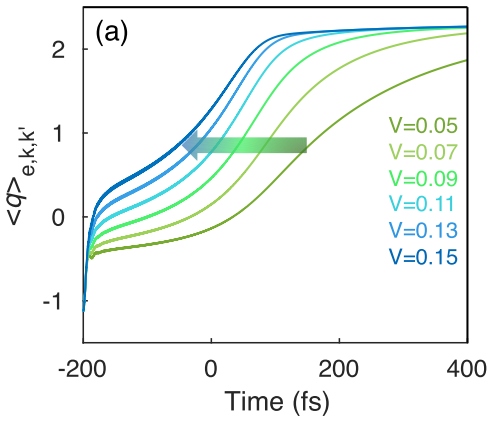

Figure 5. Proton mean position under different enol−keto electronic coupling V.

Variation of Transfer Time and Spectroscopy with System Properties

In this section, we predict how the transfer time, shape, and maximum intensity of the TRF signal of the excited-state photophysics vary with a series of system properties. The system properties include electronic coupling, H migration distance, the reactant−product energy gap, and the frequency of hydrogen stretching. Figure 6 shows predictions for the variation of features of the TRF signal of excited-state photophysics when changing system properties. Figure 6a is under the impulsive limit of the pump pulse. A striking feature includes that the keto rise becomes closer to exponential, and both the enol and keto regions show tiny oscillations. The oscillation period is ∼10 fs, meaning an OH vibrational wave packet is formed in the impulsive limit. Figure 6b lowers the vibrational dissipation rate one order of magnitude smaller and gets a transition structure on the enol decay/keto rise profile. Figure 6c combines the impulsive limit and smaller vibrational dissipation, which results in a strong oscillatory feature. The oscillation period is ∼30 fs (0.138 eV), which is around the energy gap between the first enol vibrational level and the keto level, which is closer in energy ($0.366 \times 2 - 0.61 = 0.122$ eV is their energy gap). Therefore, the oscillation is an electronic coherence feature.

Figure 6d predicts that under a smaller enol−keto gap, the enol TRF peak will be delayed and the keto signal will increase to a much higher level than the change of the enol signal. Similar trends appear when enol−keto displacement (hydrogen migration distance) is shortened (Figure 6e). This may come from an acceleration in the transition from enol to keto states. Figure 6f predicts that a smaller enol displacement compared to the ground state (i.e., the enol reorganization energy) will increase both enol and keto intensity without impacting the peak position, meaning that the ground−excited-state Franck−Condon factor is increased, the total excited-state population is increased, and the normalized enol−keto transition dynamics does not change. Overall, we attribute these signal variations to quantum mechanical transitions among ground, reactant, and product electronic states. These predictions give guidance to understanding experimental features while, at the same time, may be tested by control experiments for verification of the proposed mechanism.

https://doi.org/10.1021/acsphyschemau.2c00038
ACS Phys. Chem Au 2023, 3, 107−118

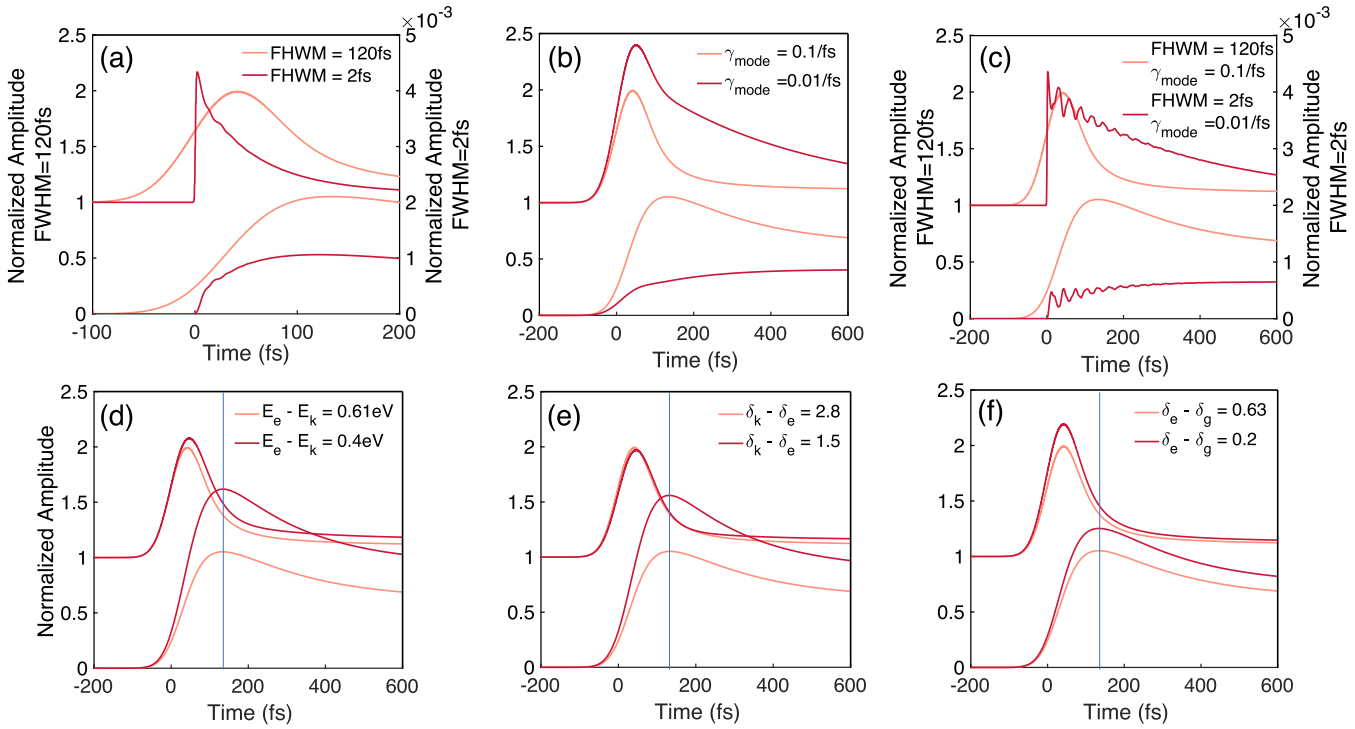

Figure 6. Predictions for variation of spectroscopy features when changing the system properties of HBT. The upper lines are 425 nm traces in the enol region, and the bottom lines are 540 nm traces in the keto region. Light red lines are the original HBT simulation in Figure 2, and deep red lines are the predictions with varying corresponding properties.

DISCUSSION

We propose a model Hamiltonian and the Lindblad master equation at modest complexity that is able to describe the ultrafast TRF signals of two ESIPT molecules, HBT and HBQ, with stable and realistic parameters, such that the theoretical model serves as a relatively reliable tool to investigate the ESIPT mechanism and predict the variation of experimental features based on system properties.

Quantitative comparison between time-resolved spectroscopy and a theoretical model is a hard problem because, from light excitation of the molecule to spectroscopy, there are many effects and motions of the degrees of freedom that take place together, with little information on how important they are and how their effects are strengthening and canceling with each other. Instead of using the detailed construction of the laser pulse, the shape of the potential energy surface, spectral density, and multiple possible vibrational modes, we model the ESIPT system using the simple master equation and spectroscopy formula as the first attempt, obtaining model parameters guided by absorption and emission spectroscopy, quantum chemistry calculation, literature, and some time-resolved data and then generalize them to describe other time-resolved data and make predictions.

The validity of the model indicates that the simple Lindblad equation, though with several microscopic assumptions, is applicable in the chemical reaction of organic chromophores in the condensed phase. It will be valuable for theorists working on quantum master equations to dig deeper into how these assumptions are valid in our examples.

CONCLUSIONS

In this work, we propose a multilevel vibronic Hamiltonian and the Lindblad master equation that is able to describe the ultrafast rise/decay profile of TRF signals of excited-state proton transfer (ESIPT) reactions of HBT and HBQ molecules. Our simulation suggests that the mechanism of ESIPT in the systems studied is an electronic population transition between enol and keto states mediated mainly by the proton coordinate rather than solely reflecting semiclassical wave packet motion. The delocalized proton wave packet evolves simultaneously with electronic dynamics and is controlled by electronic coupling between enol and keto states. The enol−keto electronic transition shows a time-dependent rate coefficient, indicating nonequilibrium quantum mechanical dynamics.

In addition, the model suggests that the absolute intensity of the TRF signal can serve as a sensitive indicator for studying isotope substitution effects. Furthermore, our model provides predictions on how the TRF signal arising from the enol and keto-dominated wavelengths varies with system properties, serving as a basis for understanding experiments and controlling ESIPT dynamics, and can be tested for the verification of the proposed proton transfer mechanism in further experiments.

Further insights into the role of the proton as opposed to skeleton modes as the dominant coordinate driving the reaction and the implications for the ultrafast optical response of ESIPT molecules could be gained by future studies that also model the skeleton modes explicitly as has been done in this work with the O−H mode. In addition, we anticipate that new experiments using the technique of 2D electronic spectroscopy together with studies that simulate the associated spectra could provide unprecedented detail about the energy structure, energy pathways, and coherences involved in ESIPT.

https://doi.org/10.1021/acsphyschemau.2c00038
ACS Phys. Chem Au 2023, 3, 107−118

■ ASSOCIATED CONTENT

Supporting Information

The Supporting Information is available free of charge at https://pubs.acs.org/doi/10.1021/acsphyschemau.2c00038.

Illustration of the ESIPT reaction of HBQ (molecular formula and diabatic potential energy surface); simulation of possible intramolecular vibrational redistribution (IVR) in HBT ESIPT reaction; proton wave packet density on enol and keto states in HBT ESIPT reaction; microscopic definition of electronic coupling; derivation of the approximated TRF formula; upper limit of H migration distance calculated by quantum chemistry; derivation of γ_{mode} for deuterated species; estimation of relaxation energy after electronic switching along skeleton mode from spectroscopy; and summary of parameter units, physical meanings, and specific values for HBT and HBQ (PDF)

Codes for reproducing density-matrix dynamics in the main text (ZIP)

■ AUTHOR INFORMATION

Corresponding Authors

Francesca Fassioli − *Department of Chemistry, Princeton University, Princeton, New Jersey 08544, United States; SISSA − Scuola Internazionale Superiore di Studi Avanzati, 34136 Trieste, TS, Italy*; Email: folsen@princeton.edu

Zhen-Su She − *Department of Mechanical and Engineering Science, Peking University, Beijing 100871, China*; Phone: +86-010-62766559; Email: she@pku.edu.cn

Gregory D. Scholes − *Department of Chemistry, Princeton University, Princeton, New Jersey 08544, United States*; orcid.org/0000-0003-3336-7960; Phone: +1-609-258-0729; Email: gscholes@princeton.edu

Authors

Luhao Zhang − *Department of Chemistry, Princeton University, Princeton, New Jersey 08544, United States*

Bo Fu − *Department of Chemistry, Princeton University, Princeton, New Jersey 08544, United States*

Complete contact information is available at: https://pubs.acs.org/10.1021/acsphyschemau.2c00038

Author Contributions

CRediT: **Luhao Zhang** writing-original draft (lead); **Francesca Fassioli** methodology (supporting), resources (equal), writing-review & editing (supporting); **Bo Fu** writing-review & editing (supporting); Gregory D. Scholes writing-review & editing (supporting); Zhen-Su She methodology (lead)

Notes

The authors declare no competing financial interest.

■ ACKNOWLEDGMENTS

The research is funded by the W. M. Keck Foundation through Award No. 1005586 and the National Natural Science Foundation of China with Grant No. 91952201. F.F. acknowledges financial support from the European Union's H2020 Maria Skłodowska Curie actions, Grant Agreement No. 799408. The authors thank Prof. Tatsushi Ikeda for suggestions on numerical coding, Dr. Rong Li for very helpful discussions, and Ben X. Z. Zhang for helpful suggestions.

■ REFERENCES

(1) Kwon, J. E.; Park, S. Y. Advanced Organic Optoelectronic Materials: Harnessing Excited-State Intramolecular Proton Transfer (ESIPT) Process. *Adv. Mater.* **2011**, *23*, 3615−3642.

(2) Zhao, J.; Ji, S.; Chen, Y.; Guo, H.; Yang, P. Excited State Intramolecular Proton Transfer (ESIPT): From Principal Photophysics to the Development of New Chromophores and Applications in Fluorescent Molecular Probes and Luminescent Materials. *Phys. Chem. Chem. Phys.* **2012**, *14*, 8803−8817.

(3) Kumpulainen, T.; Lang, B.; Rosspeintner, A.; Vauthey, E. Ultrafast Elementary Photochemical Processes of Organic Molecules in Liquid Solution. *Chem. Rev.* **2017**, *117*, 10826−10939.

(4) Daengngern, R.; Salaeh, R.; Saelee, T.; Kerdpol, K.; Kungwan, N. Excited-State Intramolecular Proton Transfer Reactions of 2,5-Bis(2′-Benzoxazolyl)Hydroquinone and Its Water Cluster Exhibiting Single and Double Proton Transfer: A TD-DFT Dynamics Simulation. *J. Mol. Liq.* **2019**, *286*, No. 110889.

(5) Tomin, V. I.; Demchenko, A. P.; Chou, P.-T. Thermodynamic vs. Kinetic Control of Excited-State Proton Transfer Reactions. *J. Photochem. Photobiol. C* **2015**, *22*, 1−18.

(6) Demchenko, A. P.; Tang, K.-C.; Chou, P.-T. Excited-State Proton Coupled Charge Transfer Modulated by Molecular Structure and Media Polarization. *Chem. Soc. Rev.* **2013**, *42*, 1379−1408.

(7) Hammes-Schiffer, S. Theory of Proton-Coupled Electron Transfer in Energy Conversion Processes. *Acc. Chem. Res.* **2009**, *42*, 1881−1889.

(8) Weinberg, D. R.; Gagliardi, C. J.; Hull, J. F.; Murphy, C. F.; Kent, C. A.; Westlake, B. C.; Paul, A.; Ess, D. H.; McCafferty, D. G.; Meyer, T. J. Proton-Coupled Electron Transfer. *Chem. Rev.* **2012**, *112*, 4016−4093.

(9) Egorova, D.; Kühl, A.; Domcke, W. Modeling of Ultrafast Electron-Transfer Dynamics: Multi-Level Redfield Theory and Validity of Approximations. *Chem. Phys.* **2001**, *268*, 105−120.

(10) Pisliakov, A. V.; Gelin, M. F.; Domcke, W. Detection of Electronic and Vibrational Coherence Effects in Electron-Transfer Systems by Femtosecond Time-Resolved Fluorescence Spectroscopy: Theoretical Aspects. *J. Phys. Chem. A* **2003**, *107*, 2657−2666.

(11) Rafiq, S.; Scholes, G. D. From Fundamental Theories to Quantum Coherences in Electron Transfer. *J. Am. Chem. Soc.* **2019**, *141*, 708−722.

(12) Kiefer, P. M.; Hynes, J. T. Theoretical Aspects of Tunneling Proton Transfer Reactions in a Polar Environment. *J. Phys. Org. Chem.* **2010**, *23*, 632−646.

(13) Kiefer, P. M.; Hynes, J. T. Kinetic Isotope Effects for Nonadiabatic Proton Transfer Reactions in a Polar Environment 1. Interpretation of Tunneling Kinetic Isotopic Effects. *J. Phys. Chem. A* **2004**, *108*, 11793−11808.

(14) Kiefer, P. M.; Hynes, J. T. Kinetic Isotope Effects for Nonadiabatic Proton Transfer Reactions in a Polar Environment. 2. Comparison with an Electronically Diabatic Description. *J. Phys. Chem. A* **2004**, *108*, 11809−11818.

(15) Agmon, N.; Gopich, I. V. Kinetic Transition in Excited-State Reversible Reactions. *Chem. Phys. Lett.* **1999**, *302*, 399−404.

(16) Solntsev, K. M.; Huppert, D.; Agmon, N. Experimental Evidence for a Kinetic Transition in Reversible Reactions. *Phys. Rev. Lett.* **2001**, *86*, 3427−3430.

(17) Lochbrunner, S.; Wurzer, A. J.; Riedle, E. Microscopic Mechanism of Ultrafast Excited-State Intramolecular Proton Transfer: A 30-Fs Study of 2-(2′-Hydroxyphenyl)Benzothiazole. *J. Phys. Chem. A* **2003**, *107*, 10580−10590.

(18) Lee, J.; Kim, C. H.; Joo, T. Active Role of Proton in Excited State Intramolecular Proton Transfer Reaction. *J. Phys. Chem. A* **2013**, *117*, 1400−1405.

(19) Takeuchi, S.; Tahara, T. Coherent Nuclear Wavepacket Motions in Ultrafast Excited-State Intramolecular Proton Transfer: Sub-30-Fs Resolved Pump−Probe Absorption Spectroscopy of 10-Hydroxybenzo[h]Quinoline in Solution. *J. Phys. Chem. A* **2005**, *109*, 10199−10207.

(20) Schriever, C.; Barbatti, M.; Stock, K.; Aquino, A. J. A.; Tunega, D.; Lochbrunner, S.; Riedle, E.; de Vivie-Riedle, R.; Lischka, H. The Interplay of Skeletal Deformations and Ultrafast Excited-State Intramolecular Proton Transfer: Experimental and Theoretical Investigation of 10-Hydroxybenzo[h]Quinoline. *Chem. Phys.* **2008**, *347*, 446−461.
(21) De Vivie-Riedle, R.; De Waele, V.; Kurtz, L.; Riedle, E. Ultrafast Excited-State Proton Transfer of 2-(2′-Hydroxyphenyl)-Benzothiazole: Theoretical Analysis of the Skeletal Deformations and the Active Vibrational Modes. *J. Phys. Chem. A* **2003**, *107*, 10591−10599.
(22) Schriever, C.; Lochbrunner, S.; Ofial, A. R.; Riedle, E. The Origin of Ultrafast Proton Transfer: Multidimensional Wave Packet Motion vs. Tunneling. *Chem. Phys. Lett.* **2011**, *503*, 61−65.
(23) Lee, S. N.; Park, J.; Lim, M.; Joo, T. Identification of an Emitting Molecular Species by Time-Resolved Fluorescence Applied to the Excited State Dynamics of Pigment Yellow 101. *Phys. Chem. Chem. Phys.* **2014**, *16*, 9394−9402.
(24) Hammes-Schiffer, S. Current Theoretical Challenges in Proton-Coupled Electron Transfer: Electron−Proton Nonadiabaticity, Proton Relays, and Ultrafast Dynamics. *J. Phys. Chem. Lett.* **2011**, *2*, 1410−1416.
(25) Hammes-Schiffer, S. Proton-Coupled Electron Transfer: Moving Together and Charging Forward. *J. Am. Chem. Soc.* **2015**, *137*, 8860−8871.
(26) Weiß, J.; May, V.; Ernsting, N. P.; Farztdinov, V.; Mühlpfordt, A. Frequency and Time-Domain Analysis of Excited-State Intramolecular Proton Transfer. Double-Proton Transfer in 2,5-Bis(2-Benzoxazolyl)-Hydroquinone? *Chem. Phys. Lett.* **2001**, *346*, 503−511.
(27) Barbatti, M.; Aquino, A. J. A.; Lischka, H.; Schriever, C.; Lochbrunner, S.; Riedle, E. Ultrafast Internal Conversion Pathway and Mechanism in 2-(2′-Hydroxyphenyl)Benzothiazole: A Case Study for Excited-State Intramolecular Proton Transfer Systems. *Phys. Chem. Chem. Phys.* **2009**, *11*, 1406−1415.
(28) Pijeau, S.; Foster, D.; Hohenstein, E. G. Excited-State Dynamics of 2-(2′-Hydroxyphenyl)Benzothiazole: Ultrafast Proton Transfer and Internal Conversion. *J. Phys. Chem. A* **2017**, *121*, 4595−4605.
(29) Higashi, M.; Saito, S. Direct Simulation of Excited-State Intramolecular Proton Transfer and Vibrational Coherence of 10-Hydroxybenzo[h]Quinoline in Solution. *J. Phys. Chem. Lett.* **2011**, *2*, 2366−2371.
(30) Nitzan, A.*Chemical Dynamics in Condensed Phases: Relaxation, Transfer and Reactions in Condensed Molecular Systems*; Oxford University Press, 2006.
(31) Breuer, H. P.; Petruccione, F.*The Theory of Open Quantum Systems*; Oxford University Press, 2007.
(32) May, V.; Kühn, O.*Charge and Energy Transfer Dynamics in Molecular Systems*; Wiley-VCH, 2011.
(33) Aly, S. M.; Usman, A.; AlZayer, M.; Hamdi, G. A.; Alarousu, E.; Mohammed, O. F. Solvent-Dependent Excited-State Hydrogen Transfer and Intersystem Crossing in 2-(2′-Hydroxyphenyl)-Benzothiazole. *J. Phys. Chem. B* **2015**, *119*, 2596−2603.
(34) Chou, P.-T.; Chen, Y.-C.; Yu, W.-S.; Chou, Y.-H.; Wei, C.-Y.; Cheng, Y.-M. Excited-State Intramolecular Proton Transfer in 10-Hydroxybenzo[h]Quinoline. *J. Phys. Chem. A* **2001**, *105*, 1731−1740.
(35) Sanz, M.; Douhal, A. Femtosecond Emission Study of H-Atom Transfer Reaction Dynamics in a New System with an Internal H-Bond. *Chem. Phys. Lett.* **2005**, *401*, 435−439.
(36) Hazra, A.; Soudackov, A. V.; Hammes-Schiffer, S. Role of Solvent Dynamics in Ultrafast Photoinduced Proton-Coupled Electron Transfer Reactions in Solution. *J. Phys. Chem. B* **2010**, *114*, 12319−12332.
(37) Fulton, R. L.; Gouterman, M. Vibronic Coupling. I. Mathematical Treatment for Two Electronic States. *J. Chem. Phys.* **1961**, *35*, 1059−1071.
(38) Piepho, S. B.; Krausz, E. R.; Schatz, P. N. Vibronic Coupling Model for Calculation of Mixed Valence Absorption Profiles. *J. Am. Chem. Soc.* **1978**, *100*, 2996−3005.
(39) Reimers, J. R.; McKemmish, L. K.; McKenzie, R. H.; Hush, N. S. Non-Adiabatic Effects in Thermochemistry, Spectroscopy and Kinetics: The General Importance of All Three Born−Oppenheimer Breakdown Corrections. *Phys. Chem. Chem. Phys.* **2015**, *17*, 24641−24665.
(40) Butkus, V.; Valkunas, L.; Abramavicius, D. Vibronic Phenomena and Exciton−Vibrational Interference in Two-Dimensional Spectra of Molecular Aggregates. *J. Chem. Phys.* **2014**, *140*, No. 034306.
(41) Fuller, F. D.; Pan, J.; Gelzinis, A.; Butkus, V.; Senlik, S. S.; Wilcox, D. E.; Yocum, C. F.; Valkunas, L.; Abramavicius, D.; Ogilvie, J. P. Vibronic Coherence in Oxygenic Photosynthesis. *Nat. Chem.* **2014**, *6*, 706−711.
(42) Dean, J. C.; Mirkovic, T.; Toa, Z. S. D.; Oblinsky, D. G.; Scholes, G. D. Vibronic Enhancement of Algae Light Harvesting. *Chem* **2016**, *1*, 858−872.
(43) Wolfseder, B.; Seidner, L.; Domcke, W.; Stock, G.; Seel, M.; Engleitner, S.; Zinth, W. Vibrational Coherence in Ultrafast Electron-Transfer Dynamics of Oxazine 1 in N,N-Dimethylaniline: Simulation of a Femtosecond Pump-Probe Experiment. *Chem. Phys.* **1998**, *233*, 323−334.
(44) Egorova, D.; Thoss, M.; Domcke, W.; Wang, H. Modeling of Ultrafast Electron-Transfer Processes: Validity of Multilevel Redfield Theory. *J. Chem. Phys.* **2003**, *119*, 2761−2773.
(45) Hazra, A.; Soudackov, A. V.; Hammes-Schiffer, S. Isotope Effects on the Nonequilibrium Dynamics of Ultrafast Photoinduced Proton-Coupled Electron Transfer Reactions in Solution. *J. Phys. Chem. Lett.* **2011**, *2*, 36−40.
(46) Lindblad, G. On the Generators of Quantum Dynamical Semigroups. *Commun. Math. Phys.* **1976**, *48*, 119−130.
(47) Brasil, C. A.; Fanchini, F. F.; Napolitano, R. J. A Simple Derivation of the Lindblad Equation. *Rev. Bras. Ensino Fís.* **2013**, *35*, 01−09.
(48) Manzano, D. A Short Introduction to the Lindblad Master Equation. *AIP Adv.* **2020**, *10*, No. 025106.
(49) Fu, B.; Hsu, L.-Y. Photoinduced Anomalous Coulomb Blockade and the Role of Triplet States in Electron Transport through an Irradiated Molecular Transistor. II. Effects of Electron-Phonon Coupling and Vibrational Relaxation. *J. Chem. Phys.* **2019**, *151*, No. 054704.
(50) Tupkary, D.; Dhar, A.; Kulkarni, M.; Purkayastha, A. Fundamental Limitations in Lindblad Descriptions of Systems Weakly Coupled to Baths. *Phys. Rev. A* **2022**, *105*, 32208.
(51) Lochbrunner, S.; Stock, K.; Riedle, E. Direct Observation of the Nuclear Motion during Ultrafast Intramolecular Proton Transfer. *J. Mol. Struct.* **2004**, *700*, 13−18.
(52) Kim, C. H.; Joo, T. Coherent Excited State Intramolecular Proton Transfer Probed by Time-Resolved Fluorescence. *Phys. Chem. Chem. Phys.* **2009**, *11*, 10266.
(53) Gelin, M. F.; Pisliakov, A. V.; Domcke, W. Time- and Frequency-Gated Spontaneous Emission as a Tool for Studying Vibrational Dynamics in the Excited State. *Phys. Rev. A* **2002**, *65*, No. 062507.
(54) Rafiq, S.; Fu, B.; Kudisch, B.; Scholes, G. D. Interplay of Vibrational Wavepackets during an Ultrafast Electron Transfer Reaction. *Nat. Chem.* **2021**, *13*, 70−76.
(55) Onuchic, J. N. Effect of Friction on Electron Transfer: The Two Reaction Coordinate Case. *J. Chem. Phys.* **1987**, *86*, 3925−3943.
(56) Yan, Y.-A. Low-Storage Runge-Kutta Method for Simulating Time-Dependent Quantum Dynamics. *Chin. J. Chem. Phys.* **2017**, *30*, 277−286.
(57) Frisch, M. J.; Trucks, G. W.; Schlegel, H. B.; Scuseria, G. E.; Robb, M. A.; Cheeseman, J. R.; Scalmani, G.; Barone, V.; Petersson, G. A.; Nakatsuji, H.; Li, X.; Caricato, M.; Marenich, A. V.; Bloino, J.; Janesko, B. G.; Gomperts, R.; Mennucci, B.; Hratch, D.*Gaussian 16*, revision C.01; Gaussian, Inc.: Wallingford, CT, 2016.
(58) Dennington, R.; Keith, T. A.; Millam, J. M.*GaussView*, version 6; Semichem Inc.: Shawnee Mission, KS, 2019.

https://doi.org/10.1021/acsphyschemau.2c00038
ACS Phys. Chem Au 2023, 3, 107−118

(59) Ernsting, N. P.; Kovalenko, S. A.; Senyushkina, T.; Saam, J.; Farztdinov, V. Wave-Packet-Assisted Decomposition of Femtosecond Transient Ultraviolet−Visible Absorption Spectra: Application to Excited-State Intramolecular Proton Transfer in Solution. *J. Phys. Chem. A* **2001**, *105*, 3443−3453.
(60) Wnuk, P.; Burdziński, G.; Sliwa, M.; Kijak, M.; Grabowska, A.; Sepioł, J.; Kubicki, J. From Ultrafast Events to Equilibrium − Uncovering the Unusual Dynamics of ESIPT Reaction: The Case of Dually Fluorescent Diethyl-2,5-(Dibenzoxazolyl)-Hydroquinone. *Phys. Chem. Chem. Phys.* **2014**, *16*, 2542.

https://doi.org/10.1021/acsphyschemau.2c00038
ACS Phys. Chem Au 2023, 3, 107−118